AN ELECTROCHEMICAL FRAMEWORK TO EXPLAIN INTERGRANULAR STRESS CORROSION CRACKING IN AN Al-5.4%Cu-0.5%Mg-0.5%Ag ALLOY

D.A. Little, B.J. Connolly, and J.R. Scully

Department of Materials Science and Engineering
Center for Electrochemical Science and Engineering
University of Virginia
Charlottesville, VA 22904-4745

Abstract

A modified version of the Cu-depletion electrochemical framework was used to explain the metallurgical factor creating intergranular stress corrosion cracking susceptibility in an aged Al-Cu-Mg-Ag alloy, C416. This framework was also used to explain the increased resistance to intergranular stress corrosion cracking in the overaged temper. Susceptibility in the underaged and T8 condition is consistent with the grain boundary Cu-depletion mechanism. Improvements in resistance of the T8 + thermal exposure of 5000 h at 225°F ($T8^{+}$) compared to the T8 condition can be explained by depletion of Cu from solid solution.

Introduction

Newer variants of precipitation age hardenable Al alloys that offer good combinations of strength-to-toughness (e.g., K_{JICi} as high as 31-37 MPa$\sqrt{m}$ [1] for a σ_{ys} of 497 MPa for C416-T8) while still maintaining or reducing weight are desirable. However, high strength precipitation age hardened alloys such as those with Cu and Mg often exhibit susceptibility to localized corrosion and stress corrosion cracking (SCC).[2]

Electrochemical-based mechanisms for intergranular corrosion (IGC) and intergranular SCC (IGSCC) of Al-Cu and Al-Cu-Mg alloys are often based on existence of a preferential anodic path along the grain boundaries.[3-10] This active region along grain boundaries is thought to be caused by either solute depleted zones or anodic precipitates.[3-10] For instance, it has been well documented that the Cu content in solid solution in Al alloys directly correlates to the pitting potential of the Al-Cu aluminum alloys.[6] Increasing the Cu content in solid solution increases the pitting potential associated with alloy matrix. However, Cu depletion at grain boundaries due to diffusion controlled precipitation and growth of Cu-containing grain boundary precipitates can then account for IGSCC susceptibility because of reduced pitting potentials in the grain boundary zone. The driving force for preferential attack of the grain boundaries can be expressed by the difference in corrosion potential between the Cu-rich matrix and the Cu depleted boundaries.

An electrochemical framework based on Cu depletion was used to explain IGC and IGSCC susceptibility as used by Muller and Galvele[6] as well as Urushino and Sugimoto[10]. Two breakdown potentials (E_{pit}) were seen in anodic scans. The most negative was attributed to Cu-depleted grain boundaries. Confirmation by electrochemical microprobe methods[11] has yet to be performed. However, by using Al-4%Cu (SHT) to simulate the matrix prior to the depletion of Cu and pure Al to simulate the maximum Cu depletion possible at the grain boundaries such a notion can be confirmed. Susceptibility was eliminated in overaged materials because E_{pit} of the Cu-bearing matrix was lowered to E_{pit} of the grain boundaries due to the depletion of solute from precipitate nucleation and growth.[6, 10] At issue is whether this model could be applied to C416. Using such a model, IGSCC susceptibility in the $T8^{+}$ condition of C416 would be eliminated if the pitting potential of the matrix were lowered to that of pure Al due to Cu depletion from the matrix since the preferential grain boundary path would be eliminated.

This study focuses on the localized corrosion and SCC resistance of an emerging, advanced Al-Cu-Mg-Ag alloy, C416 (Al-5.4%Cu-0.5%Mg-0.5%Ag-0.3%Mn), in the peak aged T8 temper and T8 + thermal exposure of 5000 h at 225°F ($T8^{+}$) conditions. It has been well documented in literature that the addition of small amount of Ag to Al-Cu-Mg alloys with high Cu:Mg ratios promotes the precipitation of thin, hexagonal shaped platelets of Ω-phase on the $\{111\}_{\alpha}$ slip planes.[1, 12-27] In the C416 alloy the θ' (Al_2Cu) and Ω (statistically equivalent to θ' in composition) precipitate phases are present on the grain boundaries and in the matrix as observed in Figure 1.[28] These precipitate phases are responsible for strengthening through precipitation age hardening.[1, 17, 29] The precipitation sequence is seen in Table I.

The T8 temper was found to be more susceptible to IGSCC than the $T8^{+}$ condition as measured by alternate immersion (AI) time-to-failure.[30, 31] The additional 5000 h of thermal treatment of this alloy at 225°F (107.2°C) was conducted to simulate the possible time of exposure to service conditions that could include elevated temperature. Reynolds and

Crooks[32] have shown only mild coarsening of the Ω-phase at the grain boundaries, using transmission electron microscopy (TEM) and differential scanning calorimetry (DSC), after an exposure of 10,000 h at 107°C. However, thermal exposure at 135°C resulted in coarsening of Ω on the grain boundaries, yielding a loss in toughness, as well as precipitation of θ' which lead to a loss of strength due to the change in strengthening precipitates.[32] Domack et al.[29] showed that the fracture mode of C416 in lab air is primarily transgranular microvoid coalescence (TG MVC) with some intergranular (IG) fracture. The percentage of the IG fracture in lab air increased as the temperature and time of the thermal exposure was increased indicative of additional grain boundary precipitation and growth.[29, 32] However, the $T8^{+}$ condition exhibited much greater time-to-failures in AI SCC testing.[31, 33]

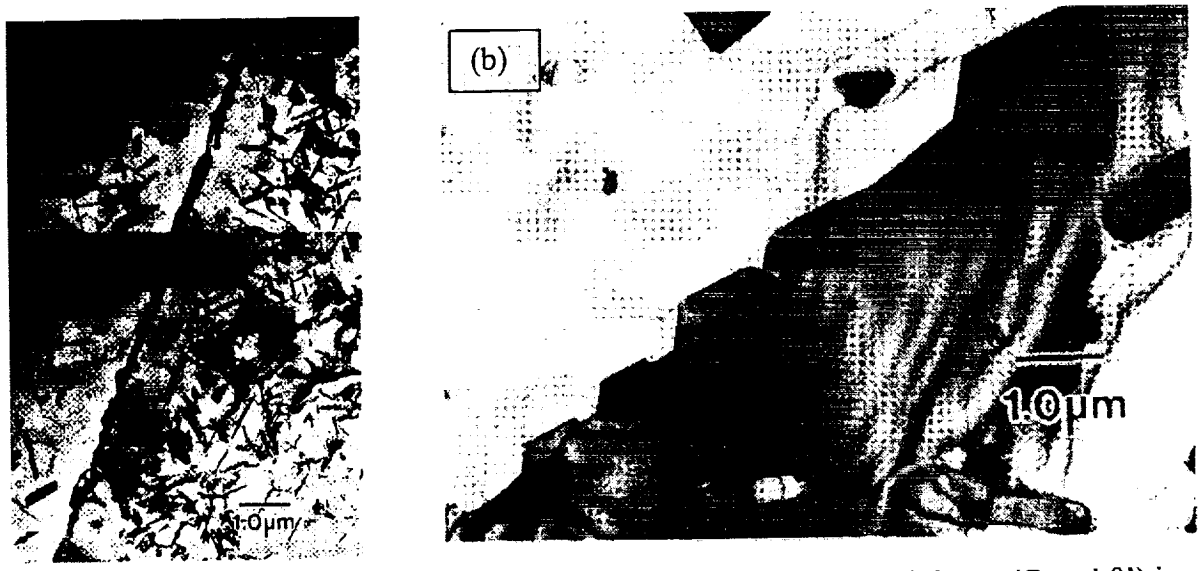

Figure 1. Transmission electron micrographs of grain boundary precipitates (Ω and θ') in an Al-4.0%Cu-0.5%Mg-0.5%Ag alloy. (a) is of a high-angle grain boundary aged for 48 h at 300°C showing a precipitate free zone which could also possibly have a solute depleted zone (e.g., Cu). (b) is of a high-angle grain boundary after 1 h at 190°C showing Ω precipitates along the grain boundary.[28]

The goals of this study are first, to define the metallurgical culprit that explains IGSCC susceptibility as a function of metallurgical condition (i.e. artificial aging time). The study seeks to confirm or refute whether the classical Cu-depletion electrochemical framework can be applied to this alloy. Second, we seek to use this electrochemical framework to help rationalize the decreases in IGSCC susceptibility upon overaging or T8 + thermal exposure (e.g., $T8^{+}$).

Experimental

The initial experiments of this study were directed at first characterizing the IGSCC or IGC susceptibility. Subsequent experiments were directed at constructing and determining consistency of data with an electrochemical framework for IGSCC based on Cu-depletion.

Material

Metallography performed on this sheet material (see Table I for composition) revealed a microstructure of equiaxed grains with diameters approximately 32-34 μm with fully

recrystallized grain structures as seen in Figure 2. C416 contains constituent particles of ~3.7 μm in size which are clearly visible at 400X magnification. These are likely Al-Cu-Mg, Al-Cu-Mn-Fe-Si, and Al-Cu-Fe phases, common to Al-Cu-Mg alloys containing Fe and Si.[8, 34-36] This alloy has a hardness of ~83.9 R_b in the T8 temper and ~84.7 R_b in the $T8^+$ condition with a Young's modulus, yield strength, and ultimate tensile strength of 71 GPa, 497 MPa, and 525 MPa respectively. Orientation imaging microscopy (OIM)[33] performed on C416-$T8^+$ revealed a wide, random distribution of grain boundary misorientations as well as a completely random crystallographic orientation distribution relative to the rolling direction, which is not the normal recrystallization texture for aluminum alloys. OIM analysis also showed that this alloy has quite a number of low angle boundaries. Low angle boundaries are typically less prone to IGC, regardless of the mechanism.[37-39] A number of different artificial heat treatments were used for these tests, these included solution heat treated (SHT) and chilled to minimize Cu-depletion from the matrix, T3 (naturally aged), underaged (UA), T8, $T8^+$, and overaged (OA) conditions. The heat treatment processes for the tempers are shown in Figure 3.

Table I. Material composition and precipitation sequence.

Material	Composition (wt%)							
	Cu	Mg	Ag	Mn	Zr	Fe	Si	Al
C416	5.4	0.5	0.5	0.3	0.13	0.06	0.04	Bal.

$\alpha_{sss} \rightarrow GP \rightarrow \theta'' \rightarrow \theta' \rightarrow \theta - (CuAl_2)$

$\alpha_{sss} \rightarrow \Omega$ (statistically equivalent to θ')

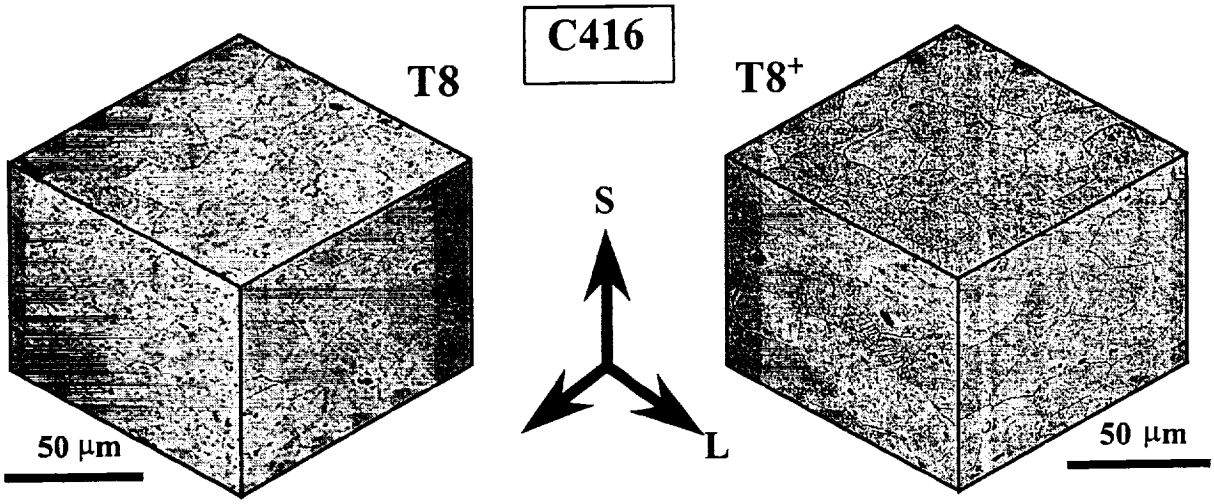

Figure 2. Three-dimensional structure section for representative C416 aluminum alloy in the T8 and T8+ conditions. (etchant used was a modified Keller's reagent)

Alternate Immersion Experiments to Define IGSCC Susceptibility

Alternate immersion (AI) tests were performed in accordance with ASTM standard G-44. Alloy C416 was tested in both the T8 and $T8^+$ tempers in order to determine and rank susceptibility to SCC. This test method shows good agreement to atmospheric tests and in-service failures.[3, 40-42] The test was performed by cyclically dunking the stressed test

coupons in the test solution (0.6 M NaCl) for 10 minutes then removing them and allowing them to dry for 50 minutes. This exposure condition was conducted with unstressed as well as stressed samples using a three-point loaded specimen jig (ASTM G-39). Serial removals and post-test examination using optical microscopy and scanning electron microscopy (SEM) was performed to determine the crack depth as a function of the exposure time and to obtain an approximate estimate on the IG crack lengths and growth rates. AI tests were also performed by NASA-LaRC[33] in the T8 and T8 + 10,000 h (@ 200°F) condition and by McDonnell Douglas[31] in the T8 and T8 + 3000 h (@ 200°F) condition as per ASTM G44 and G49 using sub-size flat tension specimens (ASTM E8) for 60 days (results shown in Figure 4).

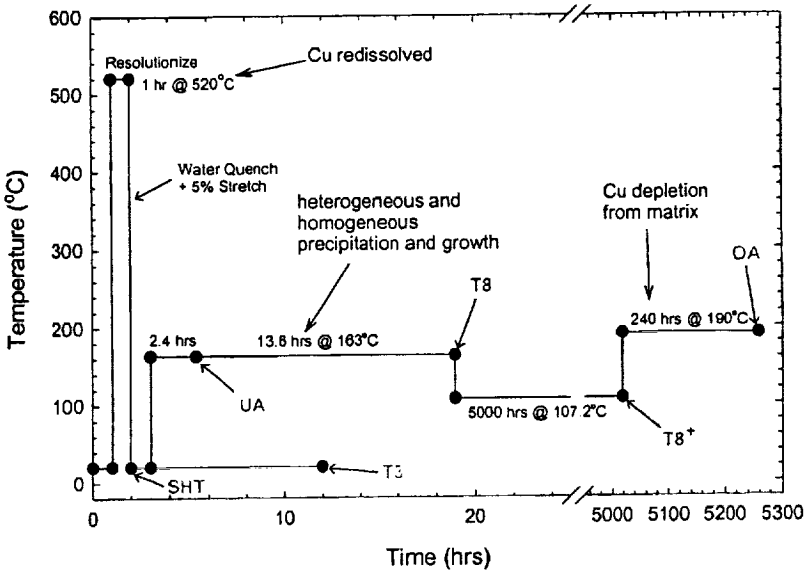

Figure 3. Heat treatment processes for the conditions (e.g. SHT, T3, UA, T8, T8$^+$, and OA) used for the various experiments performed on the alloy C416.

Pitting and Repassivation Potential Experiments to Explore Electrochemical Frameworks

In general, the critical potentials such as the pitting potential (E_{pit}) and the repassivation potential (E_{rp}) can be used to characterize the localized corrosion behavior of metals.[4, 6-8, 34, 36, 43-46] Anodic polarization scans were performed on all tempers of C416 in aerated 0.6 M NaCl (pH=7) as well as deaerated, alkaline 0.6 M NaCl (pH=10). Some example anodic polarization scans can be observed in Figure 5a. However, E_{pit} is not always an accurate measure of the resistance to pitting of an alloy, for a variety of reasons. Moreover, E_{pit} is confounded by the scan rate, oxide film thickness as well as oxide defects, at-risk surface area, and other factors.[3, 47-50] E_{rp} provides a more accurate, statistically reproducible, measure of the effects of Cu content in the matrix on dissolution properties of the alloy in pit solutions. Moreover, Connolly has observed correlation between E_{rp} and scratch repassivation potentials in Al-Li-Cu-X alloys.[51] Microstructural heterogeneity associated with intermetallic phases and solute depleted zones can confound results since each metallurgical phase has its own repassivation potential.[3, 36] Therefore, scans were also performed on synthesized θ-phase, pure aluminum (99.99%), and Al-Cu binaries (Al-0.1%Cu, Al-0.98%Cu, and Al-3.96%Cu) as models of the various components and phases of C416 to establish the electrochemical framework. Values of E_{pit} were taken as the characteristic potential where there was a permanent, significant increase in the current and increase in di/dE measured. Similarly E_{rp} was taken as the characteristic potential at which there was a significant decrease in the current and di/dE measured. An example of the determination of these critical potentials from an

anodic polarization curve is shown by Figure 5b. Figure 6 shows that like E_{pit}, E_{rp} also increases with increasing Cu content in solid solution for ~1 cm^2 surface area specimens.

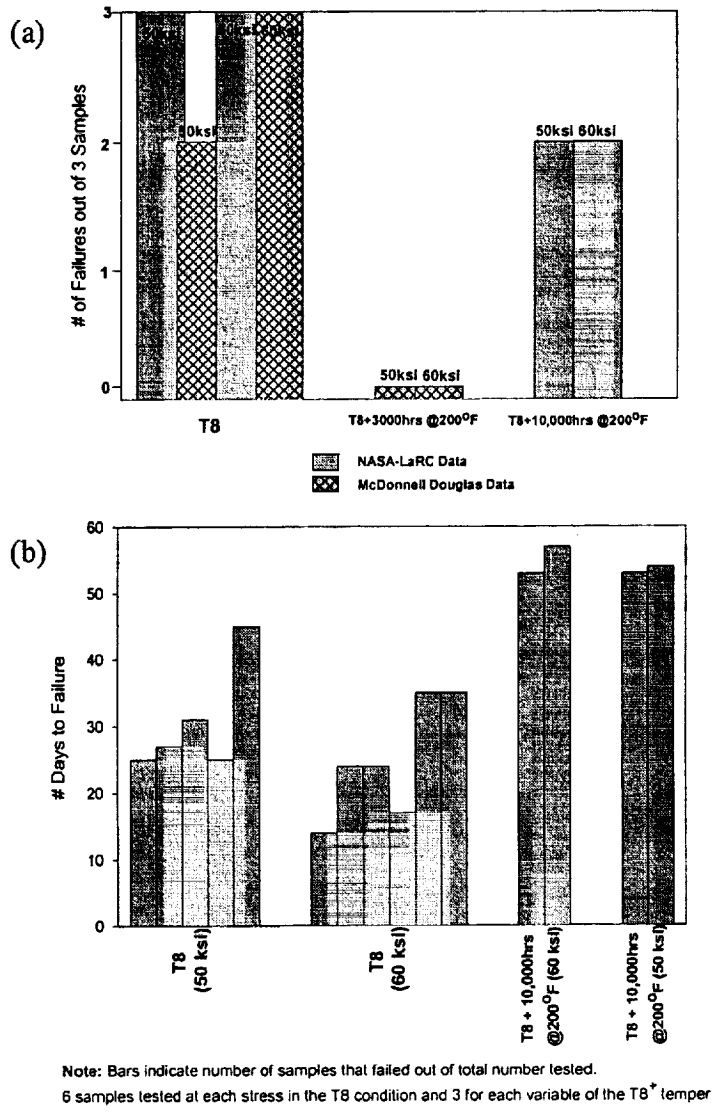

Figure 4. SCC data from AI testing conducted at NASA-LaRC and McDonnell Douglas, (a) shows the number of failures that occurred during a 60 day test for both tempers of C416 and (b) shows the number of days-to-failure for the samples that failed during the test. Note the improvement in the time-to-failure for the $T8^+$ temper as compared to that of the T8 temper.[30, 31]

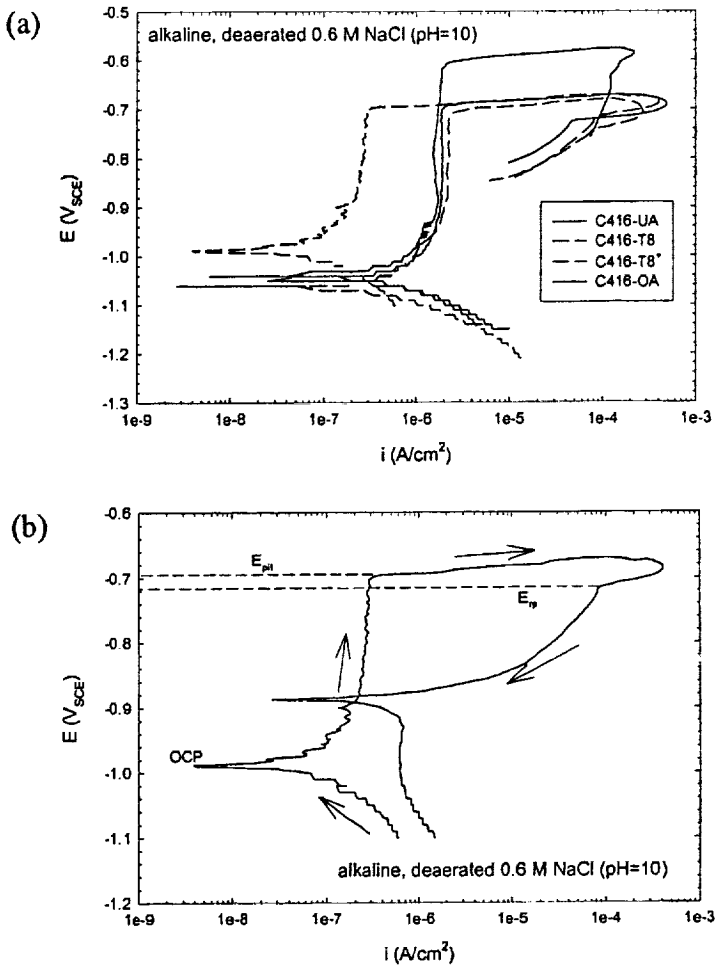

Figure 5. Anodic polarization curves in alkaline, deaerated 0.6 M NaCl (pH=10). Example curves for the UA, T8, T8+, and OA tempers of C416 are shown in (a). (b) shows where the critical potentials are located on the curves.

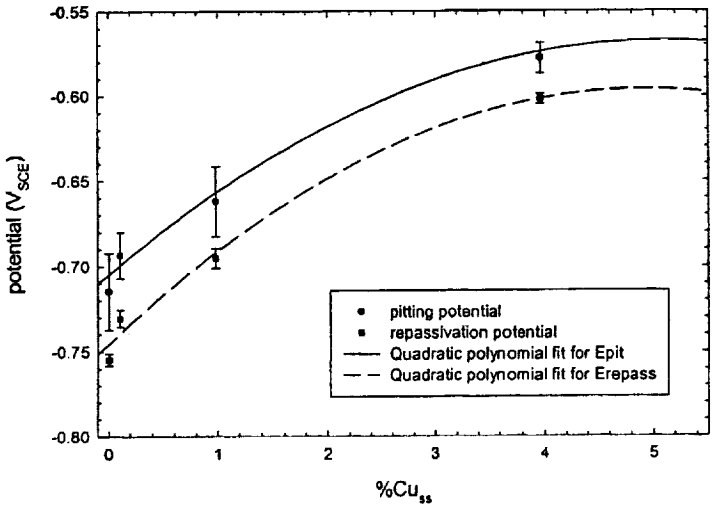

Figure 6. Pitting and repassivation potentials of SHT Al-Cu binaries as a function of %Cu in solid solution in alkaline, deaerated 0.6 M NaCl (pH=10).

Constant Extension Rate Testing (CERT) and Constant Displacement Testing

A common test method used for determining the susceptibility of materials to stress corrosion cracking is slow strain rate tensile testing (SSRT) or constant extension rate testing (CERT).[52] SSRT is a rapid test that can be used for sorting the susceptibility of Al-based materials to SCC.[53-55] There has been good correlation between the SSRT tests and the AI tests for some precipitation age hardened Al-based alloys.[53] The strain rate required for these tests is critical and most tests performed usually use a strain rate of about 10^{-6}/sec.[53-55] However, extremely slow time dependent crack growth rates will render this method ineffective for sensing IGSCC from global changes in tensile properties. CERT was performed on alloy C416 in the T8, $T8^{+}$, and UA tempers. The samples were of a tensile configuration with a thickness of ~2.2 mm, width of ~3.1 mm, and a gauge length of ~10 mm which yields a total exposed surface area of ~1 cm^2. The test environment used was an alkaline, deaerated 0.006 M NaCl solution (pH=10). This environment was selected in order to minimize pitting of the Cu-containing matrix. The sample was pre-pitted using a technique similar to an electrochemical scratch technique so that pit initiation and growth of the matrix could be initiated, propagated, and then shut off, in order to be separated and distinguished from intergranular corrosion (IGC) and intergranular stress corrosion cracking (IGSCC). Moreover, an electrochemical framework could be tested by choosing various IGSCC growth potentials. This method, which was similar to the one used by Dunn and Sridhar[56] to examine repassivation and was mentioned by Turnbull and Reid[57] involves holding the potential above the matrix pitting potential to nucleate pits (pit initiation step), then dropping the potential to just above $E_{rp\ matrix}$ to grow the pits to a particular size (pit propagation stage). Finally, the potential was set to one that is between E_{rp} of the Cu-rich matrix and E_{rp} of pure Al for the remainder of the test ($E_{rp\ Al} < E_{app} < E_{rp\ matrix}$). The general idea is that the matrix will repassivate under these conditions while the grain boundary precipitates or Al-rich grain boundary zone will continue to pit or exhibit susceptibility to IGC and IGSCC, if such an electrochemical framework applies.

X-Ray Diffraction

X-ray diffractometry (XRD) is a technique that can be used to determine the amount of solute (e.g., Cu) in solid solution in Al-based f.c.c. materials since it affects the interplanar spacing (distance between the Al solid solution crystal planes) due to its effect on the lattice parameter.[58] The change in lattice parameter is directly related to the diffraction angle (2θ) measured by the instrument through the Bragg Law.[59] The relatively random texture ensured that low index diffraction peaks could be used with reasonable reliability. This method was used to determine the relative change in the Cu concentration in solid solution for C416 in the SHT, T3, UA, T8, $T8^{+}$, and OA tempers.

Results

SCC Screening Tests

Both the T8 and $T8^{+}$ tempers of alloy C416 were susceptible to IGSCC. However, resistance to SCC expressed in terms of time-to-failure improved with the additional thermal treatment to the $T8^{+}$ temper as seen from Figure 4. Pits formed during AI started at the periphery of the bands of constituent particles that were dispersed throughout the materials and these pits began to coalesce and form larger pits. The pits formed after 10 h in alternate immersion as seen in Figure 7a and 7b clearly show an intergranular nature at their base, which also shows that this material will pit at its open circuit potential in both tempers in aerated 0.6

M NaCl solution. The results from the stressed samples show that IGC or IGSCC propagate only from pits as seen in Figure 7c. Severe pitting propagation in stressed samples obscured some of the evidence of IGSCC.

CERT tests circumvented the pit growth and coalescence stages of IGSCC and dilute Cl^- concentration as well as potential control minimized excessive pit damage. SEM performed on CERT samples reveal that the amount of IGSCC area on the fracture surface is greatest in the UA condition and is very small in the T8 and $T8^+$ condition as seen in Figure 8. The T8 temper showed small areas of IGSCC while the $T8^+$ temper revealed none. However, the primary mode of final fast failure for all tempers was by ductile microvoid coalescence. The CERT tests strongly suggest that the repassivation potential of the matrix is lowered as the artificial aging time increases from the UA to T8 to $T8^+$ temper such that the window of IGSCC susceptibility given by $E_{rp\ Al} < E_{app} < E_{rp\ matrix}$ is eliminated.

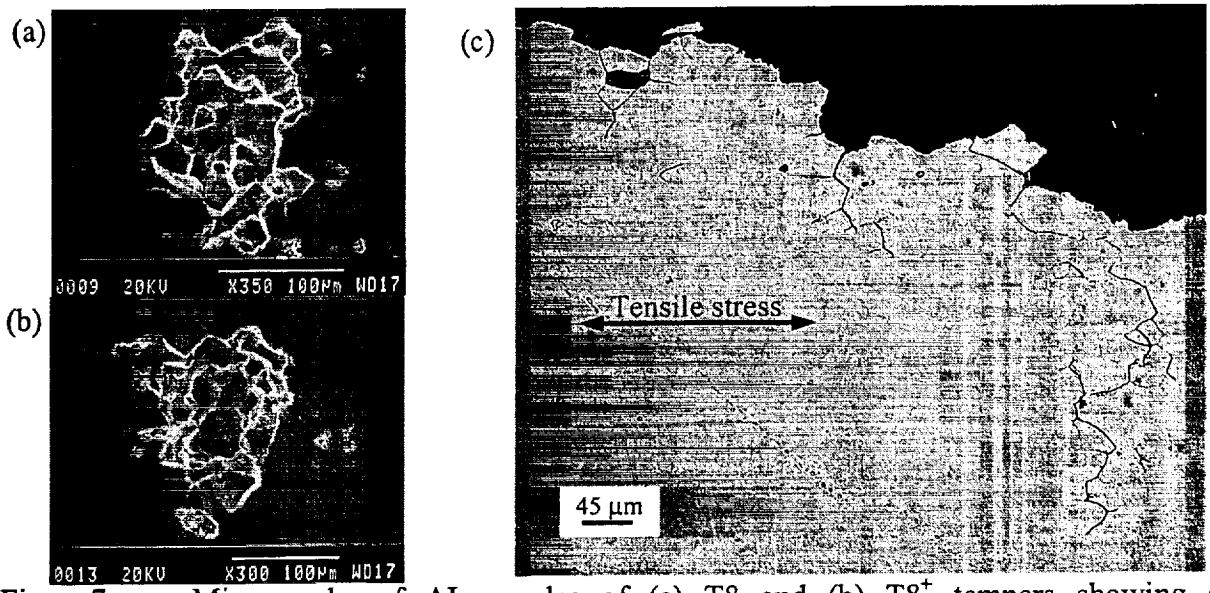

Figure 7. Micrographs of Al samples of (a) T8 and (b) $T8^+$ tempers showing an intergranular nature to the pits formed after 10 h exposure in neutral, aerated 0.6 M NaCl in unstressed condition. (c) T8 temper after 5 days exposure in the same solution under 3-pt bend stress showing IGC and IGSCC from pit sites.

Tests to Examine Cu-Depletion Framework

The first set of tests performed in the neutral, aerated 0.6 M NaCl solution revealed that C416 pits at its open circuit potential in both tempers, verifying the results observed from the alternate immersion tests. The second set of tests conducted in the alkaline, deaerated 0.6 M NaCl (pH=10) solution were done to separate pitting and repassivation potentials from the open circuit potential since pH has no effect on the pitting potential but does have one on the open circuit potential.[43, 49, 50] Two E_{rp} and two E_{pit} were not observed, which may reflect the narrow Cu-depleted zones in the alloy. Since E_{rp} was associated with large pits over a hundred times larger than any likely Cu-depleted zones it is believed they reflect the corrosion properties of the matrix. Figure 9 shows the resulting critical potentials from these anodic polarization scans conducted on the C416 alloy in the SHT, T3, UA, T8, $T8^+$, and OA tempers as well as on the synthesized bulk analogs (e.g. Al-4%Cu, Al, and θ-Al_2Cu) used as models for the components of the C416 alloy. The repassivation potential from the polarization scans correlates well with those observed from scratch repassivation tests, as seen from Figure 10a. Figure 10b shows examples of the current-time curves observed for C416-T8 held

potentiostatically at potentials above and below the potentiodynamically determined repassivation potential. Note that E_{rp} decreases as aging time increases for C416. Theta phase may dealloy but exhibits a region of passivity on upward scans over the potential range where Cu-depleted grain boundaries would corrode. Concerning the alloy, since E_{rp} is a strong function of Cu content in the Al matrix, the effect of aging on E_{rp} suggests that Cu is depleted from the matrix, as confirmed by x-ray diffraction. The reproducible E_{rp} of the T8 and T8$^+$ tempers are significantly lower than that of the Al-4%Cu (SHT) material and only slightly higher than that of the pure aluminum. As shown by Figure 11, XRD proves that Cu is significantly depleted from the matrix in the T8, T8$^+$, and OA tempers as was, also, seen electrochemically. In contrast, significant Cu is indicated in the matrix of T3, SHT, and UA alloys. Hence, the ΔE_{rp} between the possible Cu-depleted zones and matrix would be large in these tempers.

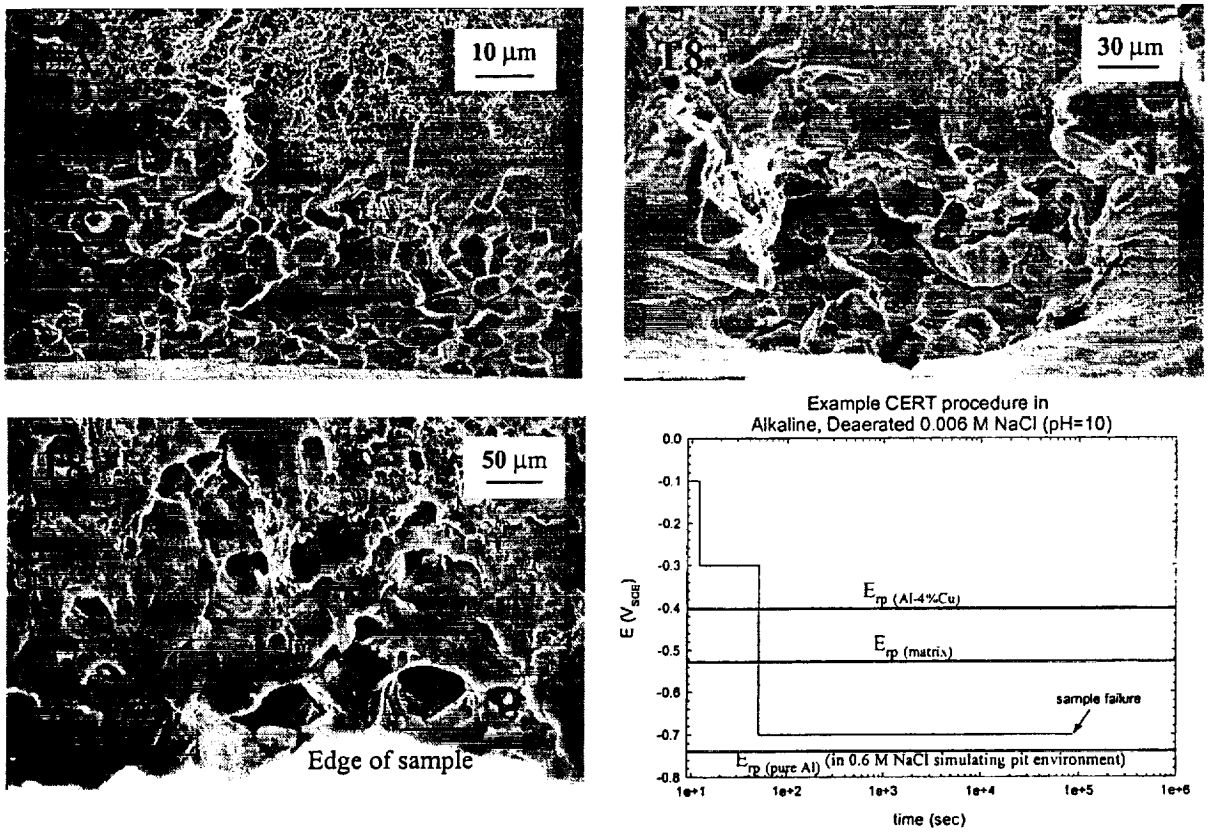

Figure 8. Micrographs of CERT samples for the UA, T8, and T8$^+$ tempers showing the effect of aging on the amount of IG fracture area along with a representation of the procedure used for the CERT tests.

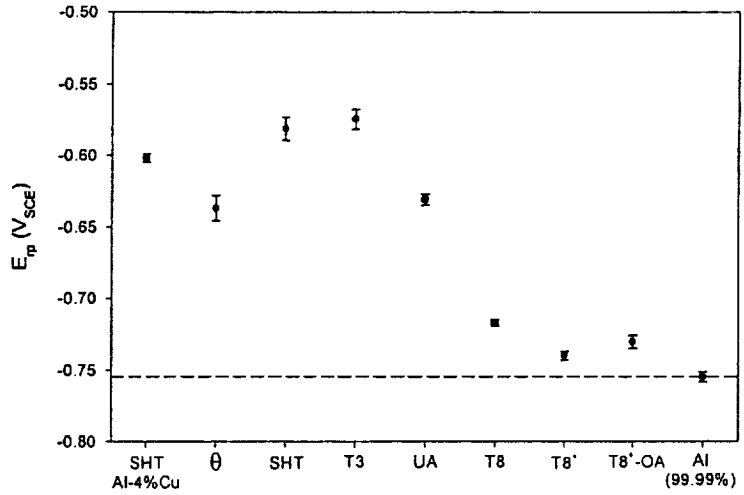

Figure 9. E_{rp} associated with the matrix of each material indicated in alkaline, deaerated 0.6 M NaCl (pH=10) for the components and tempers of C416 depicting the decrease in $\Delta E = E_{rp\ Al} - E_{rp\ matrix}$ with aging time.

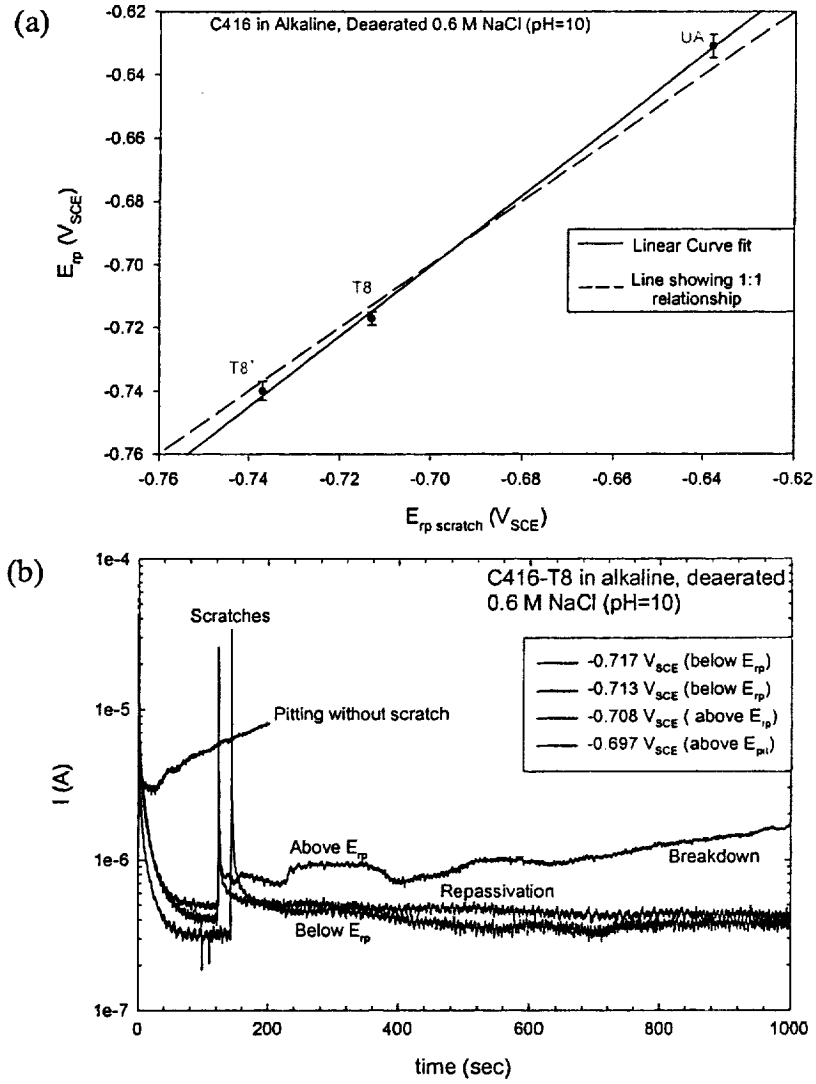

Figure 10. (a) Correlation between E_{rp} observed from the cyclic polarization scans and that observed from scratch repassivation tests. (b) Examples of current-time curves for C416-T8 held potentiostatically above and below E_{rp} as well as above E_{pit}.

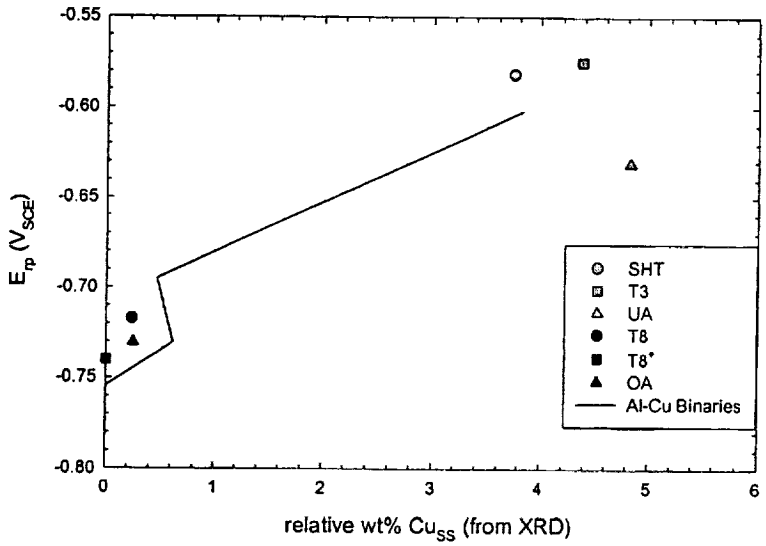

Figure 11. E_{rp} in alkaline, deaerated 0.6 M NaCl (pH=10) of C416 alloy tempers as a function of the relative %Cu in solid solution as determined from XRD indicating a Cu-depleted matrix for theT8, $T8^{+}$, and OA tempers.

Cu-Depletion Profile Calculations

Omega (Ω - Al_2Cu) precipitate size (i.e., thickness) and the associated copper solute depletion zone size along grain boundaries were modeled utilizing Zener's theory for diffusion controlled one-dimensional precipitate growth[60] as a function of artificial aging practice for aluminum alloy C416. Specifically, Zener's approximate solution was used focusing on growth due to the diffusion of super-saturated copper atoms in an aluminum matrix. All other diffusional interactions associated with and among the remaining alloying elements were ignored. The approximate solution for precipitate thickness, S, as a function of time and temperature was defined as follows:

$$S \cong \left(\frac{n_\infty - n_i}{\sqrt{n_0 - n_i}\sqrt{n_0 - n_\infty}} \right) \sqrt{Dt} \qquad (1)$$

where D is the volume diffusivity of copper atoms in an aluminum matrix, t is the aging time, n_0 is the copper concentration associated with the precipitate phase, n_i is the copper concentration associated with the matrix at the precipitate phase – matrix interface, and n_∞ is the copper concentration associated with the super-saturated aluminum matrix. Table II and Figure 12a present the calculated values for precipitate (Ω) thickness as a function of temper. The calculated values were compared with measured values obtained by Hutchison[13]. The approximate solution for maximum (Cu) solute depletion zone size, ΔS, as a function of time and temperature was defined as follows:

$$\Delta s = \frac{2(n_0 - n_\infty)S}{(n_\infty - n_i)} \qquad (2)$$

where S is the precipitate thickness, n_0 is the copper concentration associated with the precipitate phase, n_1 is the copper concentration associated with the precipitate phase – matrix interface, and n_∞ is the copper concentration associated with the super-saturated aluminum matrix. Table III and Figure 12b present the calculated maximum solute depletion zone size as a function of artificial aging time.

Copper solute concentration/depletion profiles associated with a grain boundary independent of precipitate growth were also generated utilizing solutions to the diffusion equation in a half-space with semi-infinite media. Again only copper dissolution in an aluminum matrix was considered. The solute concentration as a function of aging time and distance from the grain boundary was defined by the following equation:

$$C(x,t) = C_{grainboundary} + \left(C_{matrix} - C_{grainboundary}\right) erf\left[\frac{x}{\sqrt{4Dt}}\right] \tag{3}$$

Figure 13 presents the modeled Cu concentration profiles as a function of distance into the grain matrix from the grain boundary for an under-aged, a peak-aged, and an over-aged temper of C416. At a distance equal to ½ the Ω precipitate phases spacing substantial Cu-depletion would occur.

Table II. The Ω-phase precipitate plate thickness calculated for the UA, T8, T8$^+$, and OA tempers of C416 compared to the measured thickness for a similar alloy at various aging times.

C416 Temper	**Ω Plate Thickness Zener 1-D Growth Model Approximate Solution [60]**	**Aging Time (200 °C)** Al-4Cu-0.3Mg-0.4Ag **[13]**	**Ω Plate Thickness Measured via CTEM [13]**
UA	S = 0.93 nm	9 hours	3.6 nm
T8	S = 2.44 nm	100 hours	5 nm
T8$^+$	S = 5.80 nm	400 hours	5.68 nm
OA	S = 9.74 nm	1000 hours	7.5 nm

Table III. The maximum solute (Cu) depletion zone size calculated for the UA, T8, T8$^+$, and OA tempers of C416 compared to those calculated for a similar alloy at various aging times.

C416 Temper	**Solute Depletion Zone Maximum Size Zener 1-D Growth Model Approximate Solution [60]**	**Aging Time (200 °C)** Al-4Cu-0.3Mg-0.4Ag	**Solute Depletion Zone Maximum Size Zener 1-D Growth Model Approximate Solution [60]**
UA	ΔS = 19.4 nm	9 hours	ΔS = 75.1 nm
T8	ΔS = 44.6 nm	100 hours	ΔS = 104.3 nm
T8$^+$	ΔS = 119.8 nm	400 hours	ΔS = 118.5 nm
OA	ΔS = 203.1 nm	1000 hours	ΔS = 156.4 nm

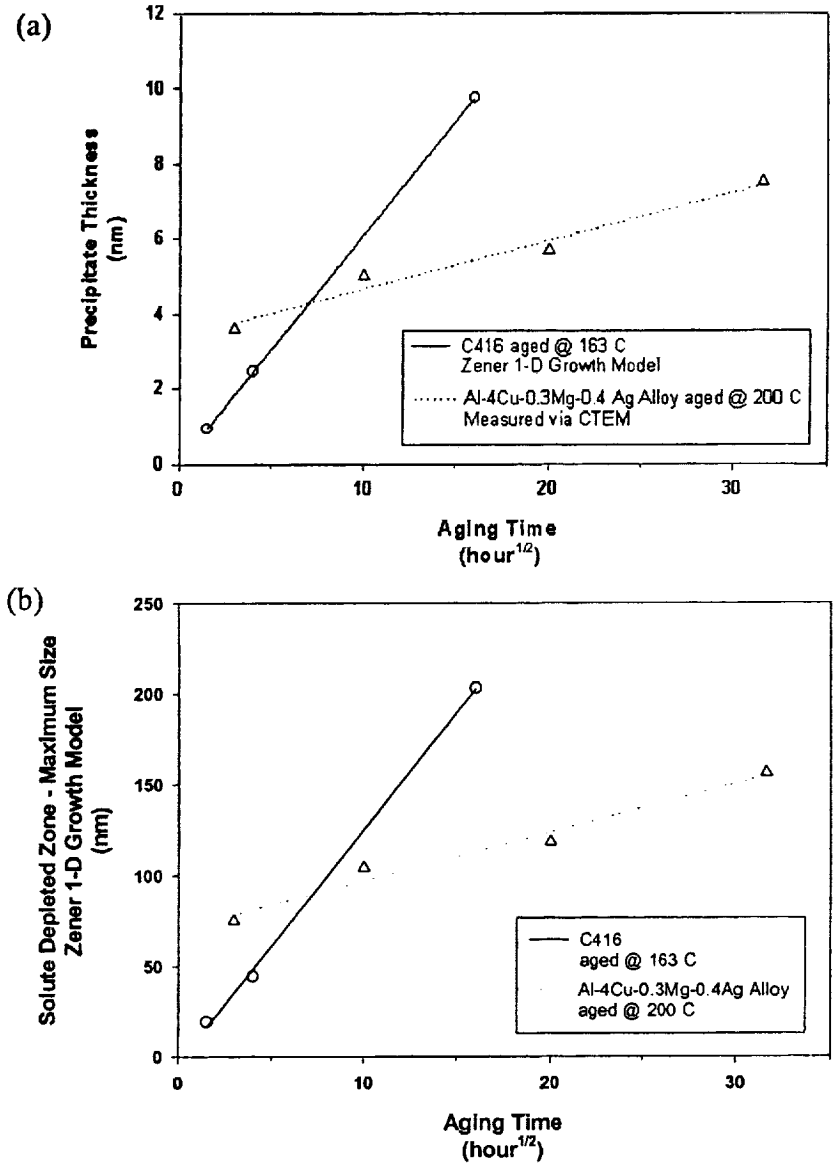

Figure 12. (a) The thickness of the Ω-phase precipitates as a function of aging time calculated for C416 (163°C) compared with the measured thickness of the precipitate in a similar alloy (200°C). (b) The calculated maximum solute (Cu) depleted zone size as a function of aging time for C416 (163°C) compared to an Al-4Cu-0.3Mg-0.4Ag alloy (200°C). Data from Tables II and III.

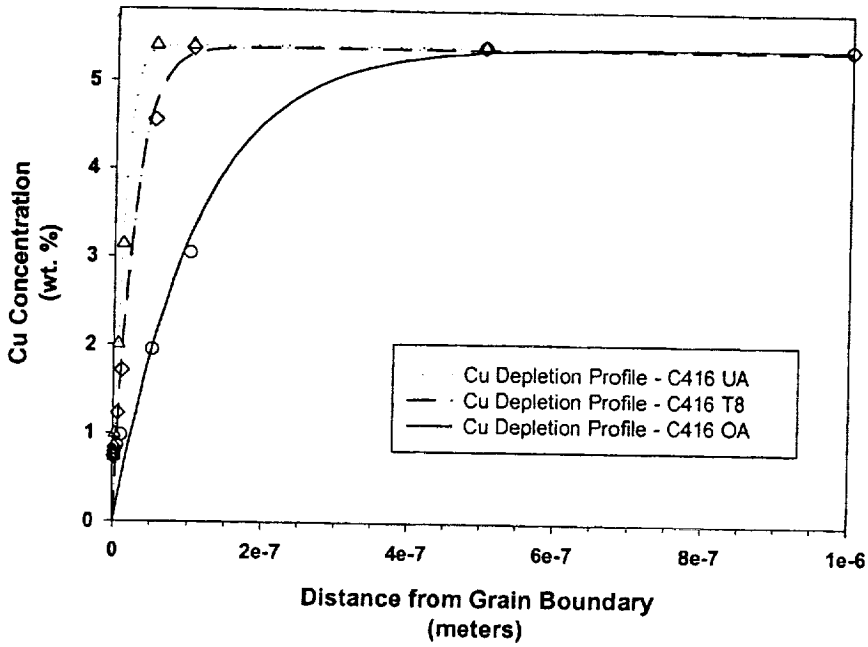

Figure 13. Cu-depletion profiles for the UA, T8, and OA tempers of alloy C416 using semi-infinite media in a half space model as described by Equation 3.

Discussion

SCC, which has been a problem since the early 1900's, requires three conditions to occur in a material: 1) an alloy with a susceptible microstructure, 2) a specific environment (e.g. saltwater), and 3) a tensile stress. Logan[42] proposed that SCC can only occur in aluminum alloys that can be strengthened by heat treatment. As was stated earlier, SCC initiates from localized corrosion sites. This is probably due to a number of reasons including; the aggressive chemistry of the pit solution and that sharp pits could be stress raisers.[57, 61] The local mechanical driving force, local environment, and local material properties all effect the transition to cracking from a pit.[57] However, this transition from localized corrosion to SCC is not yet well understood.

Al-Cu and Al-Cu-Mg alloys can exhibit a "window" of SCC susceptibility as a function of aging time, with the resistance to SCC increasing with overaging.[3, 5, 10, 62] Aging of an alloy leads to an increase in the number of precipitates and/or an increase in the volume fraction of the precipitates in the alloy matrix and along the grain boundaries. Diffusion controlled precipitation is the cause for the solute depletion that takes place in these heat treatable alloys, which in turn is consistent with the observation of IGC/IGSCC. In a solution heat treated and rapidly quenched material there is no difference in solute level between the matrix and the boundaries. However, the difference in solute levels increases after artificial aging and diffusion controlled precipitation and growth since the solute (e.g., Cu) is accumulated by the precipitates. By mass balance considerations it must be depleted from the matrix and slow Cu diffusion in Al ensures the presence of Cu-depletion. However, when the material is heat treated past the peak-aged temper the susceptibility actually decreases due to a leveling of the solute depletion profiles. The solute concentration approaches that of the level at equilibrium with Ω. This was confirmed by XRD. The difference in the amount of solute in the matrix and that along the boundaries becomes smaller as the material ages past peak strength to an OA temper, which in turn decreases the electrochemical driving force for IGC/IGSCC based on ΔE ($E_{rp\ matrix} - E_{rp\ Al}$).

The results from NASA-LaRC and McDonnell Douglas suggest that the difference in SCC susceptibility between the T8 and $T8^+$ tempers for alloy C416 is of a degree. Since both tempers pit at their open circuit potentials in the neutral Cl^- containing solution then any difference between the susceptibility to SCC is not due to the chance of forming an initial pit or the electrochemical solution used. OCP pitting prompted a change in the test environment to the alkaline, deaerated solution as a means to separate the open circuit potential from E_{pit} and E_{rp}. The results from the AI studies were most useful since it shows that the pits were necessary for IGSCC, suggesting that a specific pit chemistry is necessary to initiate IGC. This environment was reproduced in CERT experiments using an electrochemical scratch method.

Moreover, a new CERT test designed to separate pitting from IGSCC was effective in testing the validity of the well known Cu depletion framework. Specifically, susceptibility followed the order UA>T8>$T8^+$ based on % intergranular fracture after a fixed SCC test period. Decreased susceptibility correlated with decreases in ΔE ($E_{rp\ matrix} - E_{rp\ Al}$).

Conclusions

The following were conclusions were made with regard to this study:

1. An electrochemical framework based on Cu-depletion has been established to explain the change in resistance to IGSCC from the UA to the T8 to the $T8^+$ temper. Improvement in IGSCC behavior was consistent with a decrease in ΔE ($E_{rp\ matrix} - E_{rp\ Al}$) with increasing aging time.
2. The difference in IGSCC susceptibility between the two tempers, T8 and $T8^+$, of alloy C416 is more of a degree. Results are consistent with the Cu-depletion framework.

Acknowledgments

We also wish to acknowledge the support of the NASA-Langley Research Center with M. Domack as contract monitor. Equipment and instrument support at Perkin Elmer and Scribner Associates, Inc. are also gratefully acknowledged.

References

1. M.J. Haynes and R.P. Gangloff, *Elevated Temperature Fracture Toughness of Al-Cu-Mg-Ag Sheet: Characterization and Modeling.* Metallurgical and Materials Transactions A, 1997. **28A**(September): p. 1815-1829.
2. *Corrosion.* 9th ed. ASM Handbook. Vol. 13. 1992, ASM International: Metals Park, OH. 113.
3. S. Maitra and G.C. English, *Mechanism of Localized Corrosion of 7075 Alloy Plate.* Metallurgical Transactions A, 1981. **12A**(March): p. 535-541.
4. J.R. Galvele and S.M. de De Micheli, *Mechanism of Intergranular Corrosion of Al-Cu Alloys.* Corrosion Science, 1970. **10**: p. 795-807.
5. K. Sugimoto, *et al.*, *Stress Corrosion Cracking of Aged Al-4%Cu Alloy in NaCl Solution.* Corrosion Science, 1975. **15**: p. 709-720.
6. I.L. Muller and J.R. Galvele, *Pitting Potential of High Purity Binary Aluminum Alloys - I. Al-Cu Alloys. Pitting and Intergranular Corrosion.* Corrosion Science, 1977. **17**: p. 179-1936.
7. S.J. Ketcham and F.H. Haynie, *Electrochemical Behavior of Aluminum Alloys Susceptible to Intergranular Corrosion. I. Effect of Cooling Rate on Structure and Electrochemical Behavior in 2024 Aluminum Alloy.* Corrosion, 1963. **19**: p. 242t-246t.

8. V. Guillaumin and G. Mankowski, *Localized Corrosion of 2024 T351 Aluminum Alloy in Chloride Media.* Corrosion Science, 1999. **41**: p. 421-438.
9. S. Maitra and G.C. English, *Environmental Factors Affecting Localized Corrosion of 7075-T7351 Aluminum Alloy Plate.* Metallurgical Transactions A, 1982. **13A**(January): p. 161-166.
10. K. Urushino and K. Sugimoto, *Stress-Corrosion Cracking of Aged Al-Cu-Mg Alloys in NaCl Solution.* Corrosion Science, 1979. **19**: p. 225-236.
11. T. Suter and R.C. Alkire. *Microelectrochemical Studies of Pit Initiation at Single Inclusions in a 2024-T3 Al Alloy.* in *Critical Factors in Localized Corrosion III.* 1998. Boston, MA: The Electrochemical Society.
12. R.J. Chester and I.J. Polmear, *Precipitation in Al-Cu-Mg-Ag Alloys*, in *The Metallurgy of Light Alloys.* 1983, Institution of Metallurgists: London. p. 75-81.
13. C.R. Hutchinson, *et al. On the Origin of the High Resistance to Coarsening of Ω Plates in Al-Cu-Mg-(Ag) Alloys Using Z-Contrast Microscopy.* in *Aluminium Alloys Their Physical and Mechanical Properties ICAA7.* 2000. Charlottesville, VA: Trans Tech Publications Ltd.
14. Y.C. Chang and J.M. Howe, *Composition and Stability of Ω Phase in an Al-Cu-Mg-Ag Alloy.* Metallurgical Transactions A, 1993. **24A**(July): p. 1461-1470.
15. V.D. Scott, S. Kerry, and R.L. Trumper, *Nucleation and Growth of Precipitates in Al-Cu-Mg-Ag Alloys.* Materials Science and Technology, 1987. **3**(October): p. 827-835.
16. B. Skrotzki, H. Hargarter, and E.A. Starke Jr., *Microstructural Stability Under Creep Conditions of Two Al-Cu-Mg-Ag Alloys.* Materials Science Forum, 1996. **217-222**: p. 1245-1250.
17. K.M.B. Taminger, *et al. Evaluation of Creep Behavior of Emerging Aluminum Alloys for Supersonic Aircraft Applications.* in *The 6th International Conference on Aluminum Alloys.* 1998. Toyohashi, Japan.
18. I.J. Polmear, *Light Alloys: Metallurgy of the Light Metals.* 3rd ed. Metallurgy and Materials Science Series, ed. R. Honeycombe and P. Hancock. 1995, New York: Arnold.
19. J.H. Auld, *Structure of Metastable Precipitate in Some Al-Cu-Mg-Ag Alloys.* Materials Science and Technology, 1986. **2**(August): p. 784-787.
20. I.S. Suh and J.K. Park, *Influence of the Elastic Strain Energy on the Nucleation of Ω Phase in Al-Cu-Mg(-Ag) Alloys.* Scripta Metallurgica et Materialia, 1995. **33**(2): p. 205-211.
21. S.P. Ringer, *et al., Precipitate Stability in Al-Cu-Mg-Ag Alloys Aged at High Temperatures.* Acta Metall. Mater., 1994. **42**(5): p. 1715-1725.
22. S.P. Ringer, B.C. Muddle, and I.J. Polmear, *Effects of Cold Work on Precipitation in Al-Cu-Mg-(Ag) and Al-Cu-Li-(Mg-Ag) Alloys.* Metallurgical and Materials Transactions A, 1995. **26A**(July): p. 1659-1671.
23. K. Hono, T. Sakurai, and I.J. Polmear, *Pre-Precipitate Clustering in an Al-Cu-Mg-Ag Alloy.* Scripta Metallurgica et Materialia, 1994. **30**(6): p. 695-700.
24. W.A. Cassada and M.F. Bartholomeusz, *The Effect of Cu and Mg Content on Mechanical Properties of Al-Cu-Mg Alloys with and without Ag Additions.* Materials Science Forum, 1996. **217-222**: p. 1765-1770.
25. W.M. Rainforth, L.M. Rylands, and H. Jones, *Nano-Beam Analysis of Ω Precipitatesin a Al-Cu-Mg-Ag Alloy.* Scripta Materialia, 1996. **35**(2): p. 261-265.
26. Q. Li and F.E. Wawner, *Characterization of a Cubic Phase in an Al-Cu-Mg-Ag Alloy.* Journal of Materials Science, 1997. **32**: p. 5363-5370.
27. S.P. Ringer, *et al., Nucleation of Precipitates in Aged Al-Cu-Mg-(Ag) Alloys with High Cu:Mg Ratios.* Acta Materialia, 1996. **44**(5): p. 1883-1898.
28. A. Garg and J.M. Howe, *Grain Boundary Precipitation in an Al-4.0Cu-0.5Mg-0.5Ag Alloy.* Acta Metall. Mater., 1992. **40**(9): p. 2451-2462.
29. M.S. Domack, *et al. Effect of Thermal Exposure on the Strength-Toughness Behavior of Elevated Temperature Service Aluminum Alloys.* in *ICAA-6.* 1998. Toyohashi, Japan.
30. M.S. Domack, private communication with author, NASA-Langley Research Center, 1998.
31. E. Agarwal, *High Speed Research - Airframe Technology*, . 1995, McDonnell Douglas: Long Beach, CA.
32. A.P. Reynolds and R.E. Crooks, *The Effect of Thermal Exposure on the Fracture Behavior of Aluminum Alloys Intended for Elevated Temperature Service*, . 1997, ASTM: West Conshohocken, PA.
33. *Report on Two Aluminum Alloys, C415-T8$^+$ and C416-T8$^+$ Provided by the University of Virginia*, . 1999, TexSEM Laboratories, Inc.: Draper, UT.
34. R.P. Wei, C.-M. Liao, and M. Gao, *A Transmission Electron Microscopy Study of Constituent-Particle-Induced Corrosion in 7075-T6 and 2024-T3 Aluminum Alloys.* Metallurgical and Materials Transactions A, 1998. **29A**(April): p. 1153-1160.
35. M. Gao, C.R. Feng, and R.P. Wei, *An Analytical Electron Microscopy Study of Constituent Particles in Commercial 7075-T6 and 2024-T3 Alloys.* Metallurgical and Materials Transactions A, 1998. **29A**(April): p. 1145-1151.
36. G.S. Chen, M. Gao, and R.P. Wei, *Microconstituent-Induced Pitting Corrosion in Aluminum Alloy 2024-T3.* Corrosion, 1996. **52**(1): p. 8-15.
37. O.P. Arora, G.R. Ramagopal, and M. Metzger, *Grain Boundary and General Corrosion of High-Purity Aluminum in Hydrochloric Acid.* Transactions of Metallurgical Society of AIME, 1962. **224**(June): p. 541-549.

38. O.P. Arora and M. Metzger, *Corrosion of Some Tilt and Twist Boundaries in Aluminum Bicrystals.* Transactions of the Metallurgical Society of AIME, 1966. **236**(August): p. 1205-1212.
39. J.R. Scully, *Environmentally-Assisted Intergranular Cracking*, in *Materials Research Society Bulletin.* 1999. p. 36-42.
40. W.W. Binger, E.H. Hollingsworth, and D.O. Sprowls, *Ch 7. Resistance to Corrosion and Stress Corrosion*, in *Properties and Physical Metallurgy.* p. 209-276.
41. E.H. Hollingsworth and H.Y. Hunsicker, *Corrosion of Aluminum and Aluminum Alloys*, in *Metals Handbok Ninth Edition - Volume 13 Corrosion*, J.R. Davis, *et al.*, Editors. 1987, ASM International: Metals Park, Ohio. p. 583-609.
42. H.L. Logan, *The Stress Corrosion of Metals.* 1966, New York, NY: John Wiley & Sons, Inc.
43. J.R. Scully, *et al.*, *Electrochemical Characteristics of the Al_2Cu, Al_3Ta and Al_3Zr Intermetallic Phases and Their Relevancy to the Localized Corrosion of Al Alloys.* Corrosion Science, 1993. **35**(1-4): p. 185-195.
44. J. Zahavi and M. Rotel. *Corrosion Behavior of Al-Cu Alloy Thin Films in Microelectronics.* in *I. Corrosion Congress.* 1984. Toronto, Canada.
45. R.G. Buchheit, *The Electrochemistry of θ (Al_2Cu), S (Al_2CuMg) and T_1 (Al_2CuLi) and localized Corrosion and Environment Assisted Cracking in High Strength Al Alloys.* in *Aluminum Alloys - Their Physical and Mechanical Properties ICAA7.* 2000. Charlottesville, VA: Trans Tech Publications Ltd.
46. C.-M. Liao, *et al.*, *In-Situ Monitoring of Pitting Corrosion in Aluminum Alloy 2024.* Corrosion, 1998. **54**(6): p. 451-458.
47. S.T. Pride, J.R. Scully, and J.L. Hudson, *Metastable Pitting of Aluminum and Criteria for the Transition to Stable Pit Growth.* Journal of Electrochemical Society, 1994. **141**(11): p. 3028-3040.
48. J.E. Sweitzer, *Localized Corrosion Resistance of $Al_{90}Fe_5Gd_5$ and $Al_{87}Ni_{8.7}Y_{4.3}$ Alloys*, (M.S. thesis in Material Science and Engineering), University of Virginia: Charlottesville, VA, 1998, p. 27.
49. Z. Szklarska-Smialowska, *Pitting Corrosion of Metals.* 1986, Houston, TX: National Association of Corrosion Engineers. 377-399.
50. E. McCafferty, *The Electrode Kinetics of Pit Initiation on Aluminum.* Corrosion Science, 1995. **37**(3): p. 481-492.
51. B.J. Connolly, private communication, University of Virginia, 2000.
52. R.N. Parkins, *Inhibition in the Context of Environment-Sensitive Cracking*, in *Reviews on Corrosion Inhibitor Science and Technology.* 1993, National Association of Corrosion Engineers: Houston, TX. p. 1-14.
53. S. Maitra, *Determination of Stress Corrosion Cracking Resistance of Al-Cu-Mg Alloys by Slow Strain Rate and Alternate Immersion Testing.* Corrosion, 1981. **37**(2): p. 98-103.
54. H. Buhl, *Validity of the Slow Straining Test Method in the Stress Corrosion Cracking Research Compared with Conventional Techniques.* Stress Corrosion Cracking - the Slow Strain-Rate Technique, ASTM STP 665, 1979: p. 333-346.
55. G.M. Ugiansky, *et al.*, *Slow Strain-Rate Stress Corrosion Testing of Aluminum Alloys.* Stress Corrosion Cracking - the Slow Strain-Rate Technique, ASTM STP 665, 1979: p. 254-265.
56. D. Dunn and N. Sridhar. *Investigation of Processes Related to the Growth and Repassivation of Localized Corrosion of Fe-Ni-Cr-Mo Alloys.* in *Critical Factors In Localized Corrosion II.* 1995. Chicago, IL: The Electrochemical Society.
57. A. Turnbull and T.A. Reid, *Environment Assisted Cracking from Pits - A Review of Life Prediction Methodologies*, . 1999, National Physical Laboratory: Teddington, Middlesex, UK.
58. J.E. Hatch, ed., *Aluminum - Properties and Physical Metallurgy.* . 1984, American Society for Metals: Metals Park, OH. 29.
59. B.D. Cullity, *Elements of X-Ray Diffraction.* 2nd ed. 1978, Reading, MA: Addison-Wesley Publishing Company, Inc.
60. C. Zener, *Theory of Growth of Spherical Precipitates from Solid Solution.* Journal of Applied Physics, 1949. **20**(October): p. 950-953.
61. T.P. Hoar, *Electrochemical Techniques in Stress-Corrosion Cracking.* in *Recent Advances in Stress Corrosion.* 1961. Stockholm: Korrosionsnamnd.
62. D.O. Sprowls and R.H. Brown, *International Conference on Fundamental Aspects of Stress-Corrosion Cracking*, , R.W. Stahle, Editor. 1969, NACE: Houston. p. 466-512.